




Ultrasound Sensitive Smart Polyvinyl Alcohol/Melamine/Tannic Acid Hydrogel

Ş. Balcı^{1,2} · Y. Camcı^{2,3} · S. Türk^{2,4} · İ. Altınsoy⁵ · G. Çelebi Efe⁶ · M. Ipek⁵ · M. Özacar^{2,7} · C. Bindal^{2,5} 

Received: 1 July 2023 / Accepted: 19 November 2023
© King Fahd University of Petroleum & Minerals 2023

Abstract

Problems such as hydrophilic properties of hydrogels, limited encapsulation of hydrophilic drugs, and unintended release amounts damage normal tissues and lead to overdose or repeated doses. This study investigates the development and characterization of drug carrier hydrogel formulations that can protect normal tissues. In this study, polyvinyl alcohol (PVA) hydrogel was synthesized by adding melamine (M) and tannic acid (TA) at different weight ratios to limit the hydrophilic properties of the hydrogel. In the analysis of the synthesized hydrogel, the efficiency of drug encapsulation increased from 60 to 90% as the TA content increased. The degree of swelling decreased from 73 to 63%. The contact angle increased from 10.15° to 62.27°, and the surface energy decreased. Drug release analysis was performed both in the presence of ultrasound (US) in a 40 kHz ultrasonic bath at 22 °C and without US at room temperature (22 °C). The drug release of Dox-loaded hydrogels was carried out in deionized water. Hydrogels release about two times more drug under ultrasound. After TA was added to the hydrogel, the drug release decreased by about 1.5 times. Successful results have been obtained with US, which is used to increase the amount of drug in the targeted area in a short time, accelerate the effect of the drug, and get faster results. The findings obtained as a result of all these characterizations and supported by FTIR provide promising contributions for controlled drug delivery systems.

Keywords Hydrogel · Tannic acid · Ultrasound · Drug release

✉ C. Bindal
bindal@sakarya.edu.tr

¹ Biomedical Engineering, Institute of Natural Sciences, Sakarya University, Esentepe Campus, 54187 Sakarya, Turkey

² Biomaterials, Energy, Photocatalysis, Enzyme Technology, Nano & Advanced Materials, Additive Manufacturing, Environmental Applications and Sustainably Research & Development Group (BIOENAMS R&D Group), 54187 Sakarya, Turkey

³ Department of Biomedical Engineering, Pamukkale University, 20160 Denizli, Turkey

⁴ Biomedical, Magnetic and Semi Conductive Materials Research Center (BIMAS-RC), Sakarya University, Esentepe Campus, 54187 Sakarya, Turkey

⁵ Department of Metallurgy and Materials Engineering, Faculty of Engineering, Sakarya University, Esentepe Campus, 54187 Sakarya, Turkey

⁶ Faculty of Technology, Metallurgical and Materials Engineering, Sakarya University of Applied Sciences, Esentepe Campus, 54187 Sakarya, Turkey

1 Introduction

Pharmaceutical scientific research is contributing to the development of new drug delivery systems for various therapeutic agents every day. Hydrogels are favored for their properties that are very similar to those of living tissues, such as high-water content and biocompatibility. They can also be a superior option for drug delivery systems to reduce the frequency and severity of unintended releases or toxic effects associated with chemotherapeutic drug treatment [1]. However, their limited carrying capacity and rapid release have hindered their effectiveness [2]. To achieve the desired dosage and time, the structural features of the hydrogel matrix can be optimized to better regulate the release rate and duration [3].

Polyvinyl alcohol (PVA) is widely used in hydrogel-based drug carrier systems. It is preferred due to its advantageous properties such as high hydrophilicity, swelling capacity,

⁷ Department of Chemistry, Science & Arts Faculty, Sakarya University, Sakarya 54187, Turkey



water solubility, non-toxicity, biocompatibility, and flexibility [4].

Doxorubicin (DOX-HCl) is an anticancer drug used in the treatment of diseases such as leukemia, especially late-stage breast cancer and ovarian cancer [5]. The high water content of most hydrogels, i.e., hydrophilicity, results in relatively rapid release of drugs from the gel matrix over hours or days in the case of hydrophilic drugs, where the hydrogel is also typically applied in delivery. This release profile can be reduced by increasing the interactions between the drug and the hydrogel matrix when using polymers that become more hydrophobic by limiting the hydrophilic properties of the hydrogel and/or by increasing the diffusivity barrier for drug release from the hydrogel [6]. For example, hydrophilic drugs such as DOX-HCl and ciprofloxacin face challenges when delivered in a PVA hydrogel-based drug delivery system due to inadequate drug encapsulation and undesirable release kinetics and times [7]. The unintended timed release of DOX-HCl has adverse side effects on normal tissues. This limits the use of DOX-HCl in conventional free drug therapy [8].

PVA hydrogel can be improved by the application of a strong crosslinking agent to ameliorate the problems of limited encapsulation and unwanted drug release and quantity. The hydrogel created through crosslinking offers more porosity. Therefore, the encapsulation efficiency of the desired dose can be increased and drug release at an undesired time can be reduced. Materials such as M and TA can be preferred as crosslinking agents [9]. Thus, the crosslink density of the hydrogel is increased and its contact with water is reduced by the bonds formed. The hydrophilic properties of the hydrogel, whose contact with water is reduced, are limited and the drug encapsulation ability is increased. TA is a natural polyphenol widely used in pharmaceuticals, biomedical applications, drug delivery strategies, food, and medicine. TA is a natural polyphenol widely used in pharmaceuticals, biomedical applications, drug delivery strategies, food, and medicine [10]. It has remarkable properties such as anti-inflammatory, antibacterial, and anticancer activity, negligible toxicity, water solubility, and biodegradability. The utilization of TA is based on the substance's abundance of hydroxyl groups and propensity to create hydrogen bonds with biomaterials. It has drawn interest as a potential natural crosslinking agent in hydrogel and polymer biomaterials because of its capacity to generate multiple hydrogen bonding connections with a range of molecules. TA has been used to improve the properties of existing natural and synthetic biomaterials [11].

Physical interactions can result in the formation of hydrogel cross-links. These physical contacts can be electrostatic interactions, hydrophobic interactions, van der Waals bonds, hydrogen bonds, ionic interactions, crystallization, or a

mixture of these interactions [12]. For a reliable drug delivery system, these physical interactions can be adjusted in response to environmental cues. In particular, the swelling and non-swelling behaviors of smart hydrogels make them perfect as a trigger that releases medications in response to environmental conditions [13].

Thanks to the porous structure of the hydrogel created by physical interactions, it can be manipulated by means of a chemical trigger or physical energy (pH, temperature, solution concentration, solvent type, light, UV radiation, electric field strength, magnetic field strength, etc.). A manipulable smart hydrogel enables controlled drug release based on the diffusion parameter, allowing the drug to be released at a specific rate. Thus, the amount of drug released can be increased in a short time, and faster results can be achieved by accelerating the effect of the drug.

US is a highly effective physical system for controlling the spatial and temporal distribution of on-demand drug delivery [14]. US is an easy-to-use technique with no negative side effects. For example, magnetic field is inconvenient for people with pacemakers, but US is harmless. Ultrasonic energy is ideal for remotely controlling drug release and activation, preventing pharmacologic toxicity from damaging healthy tissues.

Despite numerous studies on ultrasound-triggered drug release mechanisms, they remain uncertain and not fully understood. However, the physiological effects of ultrasound application on stimulus-sensitive hydrogels can be grouped into thermal (hyperthermia) and mechanical (non-thermal) effects. In the thermal effect, as the US energy is absorbed by the tissue, heat energy is released. The amount of heat produced varies depending on the absorption capacity of the tissue, the application time, the dose, and the application method. The effect of hyperthermia leads to disruption of the cell membrane and increased permeability of blood vessels. High-intensity focused ultrasound (HIFU) can be used to trigger hyperthermia. HIFU can lead to a rapid local temperature rise and cause unpredictable and irreversible damage. In the non-thermal effect, acoustic energy is transferred into mechanical energy in the form of oscillation and force. In cavitation, which results from mechanical action, a distinction can be made between inert (due to rapid growth and collapse of microbubbles) and stable (due to continuous release of microbubbles) actions. Inertial cavitation (or temporary cavitation) occurs when the intensity of US is high enough to cause rapid growth and collapse of microbubbles. The collapse of bubbles creates shear stress, which generates shock waves. Shock waves can increase the permeability of cell membranes and blood vessels, so they can also be used for drugs that cross the blood–brain barrier (BBB) to treat diseases of the central nervous system [15]. Low-frequency ultrasound (LFUS) (30 kHz to 300 kHz) is commonly used for the sustained release of microbubbles in stable cavitation.



The sustained release of microbubbles generates velocities in the fluid that cause shear stresses that affect the release of the encapsulated drug [16]. Stable cavitation is thought to break up the cross-links of the hydrogel, and this break-up increases the size of the pores in the hydrogel, temporarily changing its characteristic diffusion properties and increasing drug release [17, 18].

US-triggered drug release is much faster than others [19]. In this study, it was aimed to synthesize hydrogels with good stability by adding TA as a second cross-linking agent in addition to M cross-linker to PVA hydrogel and to increase the drug release efficiency by affecting the cross-links formed in the hydrogel with US. Since there are very few studies on this subject in the open literature indicating the original location of the study, it was aimed to investigate the effect of TA and M. The advantage of this study is that the hydrogels developed with TA can contribute to the pharmacological field by affecting the safe transportation of harmful drugs such as DOX-HCl and the efficiency of drug release by ultrasound at the desired time.

2 Materials and Methods

2.1 Raw Materials Used in the Hydrogel

In this work, PVA (Polyvinyl Alcohol, Alfa Aesar®, 98–99% hydrolyzed, highmolecular weight, CAS: 9002–89-5), M (Melamine(2,4,6-triamino-1,3,5-triazine), Sigma-Aldrich®, %99 hydrolyzed, $M_w = 126,12$ g/mol, $d: 1,57$ g/cm³, CAS: 108–78-1), and TA (Tannic acid powder, Merck, Emprove®), NaCl (Sodium Chloride, Merck, CAS: 7647–14-5), NaHCO₃ (Sodium hydrogen carbonate, Sigma Aldrich, CAS: 144–55–8), K₂HPO₄·3H₂O (Potassium Hydrogen Phosphate Trihydrate, Merck, CAS: 16,788–57-1), KCl (Potassium Chloride, Sigma Aldrich, CAS: 7447–40-7), MgCl₂·6H₂O (Magnesium Chloride Hexahydrate, Merck, CAS: 7791–18-6), CaCl₂ (Calcium Chloride, Merck, CAS: 10,043–52-4), Na₂SO₄ (Sodium Sulfate, Merck, CAS: 7757–82-6), TRIS [Trishydroxymethyl Aminomethane, (CH₂OH)₃CNH₂, Sigma Aldrich, CAS: 77–86-1], HCl (Hydrochloric Acid, %37, Sigma Aldrich) were used as received.

2.2 Preparation of PVA, M, and TA-Enhanced Hydrogel

To prepare the final hydrogel solution, 35%(w/v) PVA and 1.5%(w/w) M precursors were prepared in 40 ml deionized water and mixed at 90 °C until the solution was homogeneous. Melamine was used to increase the cross-linking density. 0, 5, 10, and 15wt.% TA was added to separate solutions; then, the solutions were transferred into Petri dishes.

The prepared solution systems were sealed with paraffin to preclude water evaporation. For the freezing/thawing process, the hydrogels were cooled to – 20 °C for 30 min and then thawed at room temperature for at least 6 h. The freezing/thawing process was carried out several times in all. The freeze–thaw process is a type of physical crosslinking method that uses the crystallization process of precursor solutions and hydrogen bonding interactions between polymer chains to produce hydrogels [20]. It has been shown that denser and stronger structures are observed after the freeze–thaw cycle [21, 22]. The mechanism of hydrogel formation is shown in Fig. 1.

2.3 Swelling Measurements

The equilibrium swelling test was performed to examine the degree of swelling of hydrogels. The hydrogels swell by absorbing water and pores are formed where the substance in the hydrogel matrix, drug etc., can be released [23]. Hydrogel samples were dried by lyophilization, and each sample was cut into equal volume and weight (± 0.2 mg). A precision balance determined the weights of the dried hydrogel samples. Hydrogels were placed in falcon tubes containing deionized water. Hydrogels were weighed at certain time intervals at room temperature. Weighing continued until the mass values of the hydrogels did not vary with time. The degree of equilibrium swelling at different time intervals was calculated from the following Eq. (1) [24, 25].

$$\text{ESD}(\%) = \frac{W_s - W_d}{W_d} \times 100 \quad (1)$$

where W_s is the weight of swollen hydrogel samples at time intervals and W_d is the weight of dried ones.

2.4 DOX-HCl Loading and the Encapsulation Efficiency (EE%) on Hydrogel Pieces

In order to drug load, the hydrogels were submerged in 100 mL of 200 ppm DOX-HCl solution for three days at 22 °C and shaken at 200 rpm [23]. The hydrogels were removed from the solution and the amount of supernatant remaining in the solutions was determined. To determine the encapsulation efficiency (EE%), the absorbance of supernatant after DOX-HCl loading was measured at 480 nm wavelength using UV–Vis spectrophotometer (Shimadzu-2600). The amount of DOX was determined using an appropriate calibration curve of known concentrations of the drug in distilled water. The encapsulation efficiency (EE) was calculated according to Eq. (2) as in the referenced studies [26–28].

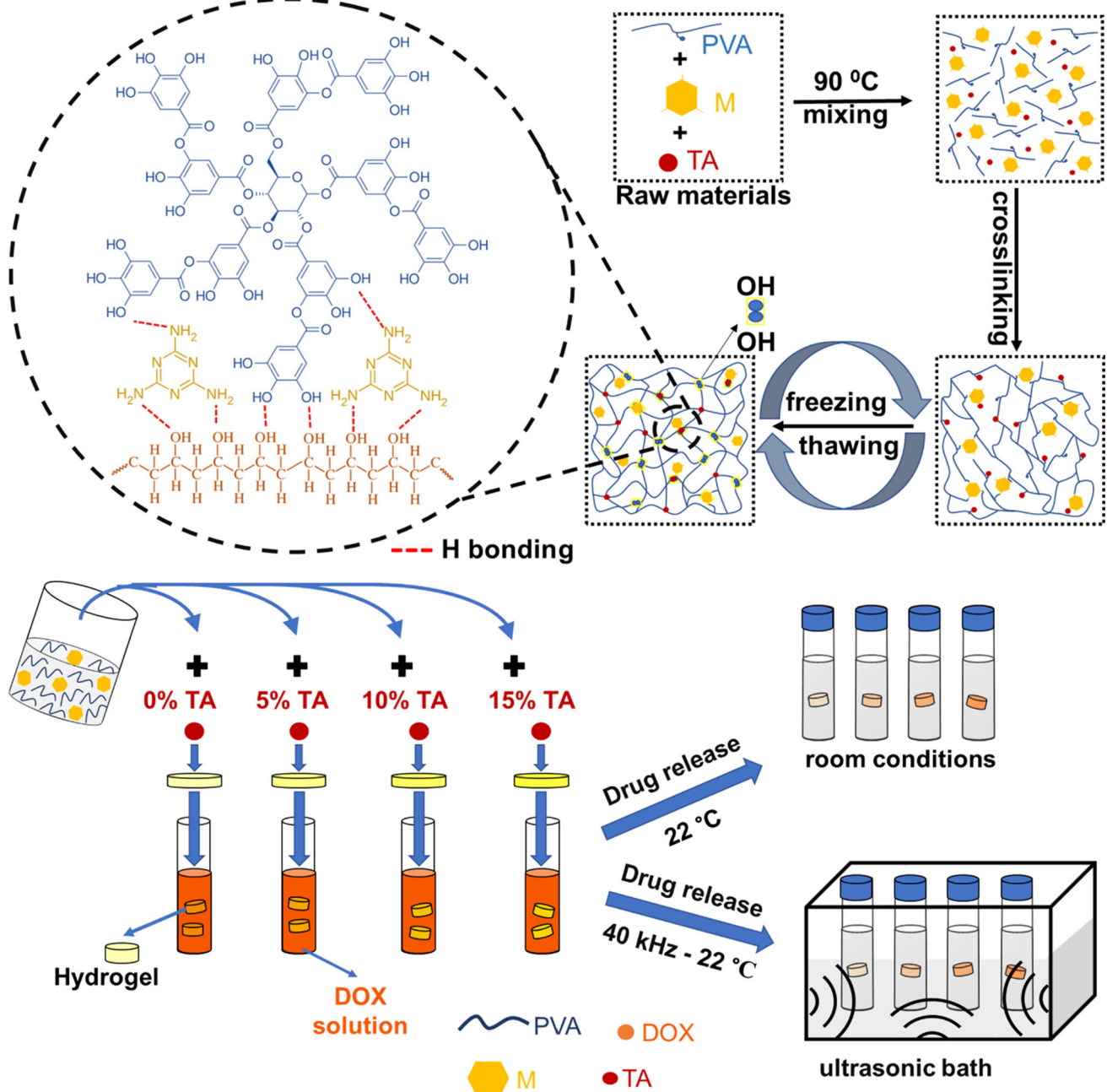


Fig. 1 Hydrogel formation mechanism, preparation process and drug release illustration

$$\text{Encapsulation efficiency (EE\%)} = \frac{(\text{Total drug} - \text{Free drug})}{\text{Total drug}} \times 100 \quad (2)$$

2.5 Drug Release Measurement of DOX-Loaded Hydrogel

Drug release of DOX-loaded hydrogels was performed at 40 kHz with an ultrasonic bath (ISOLAB) in tubes containing 5 mL of deionized water. Samples were taken from the

tubes at 15-min intervals to determine the amount of DOX released. To determine the amount of DOX released, samples were taken from the tubes at 15-min intervals. The drug concentration in each sample was measured using a UV spectrophotometer at 480 nm and calculated by summing over 15–30–45–60 min. In order to keep the liquid volume in the tube constant, after the samples were taken, all the remaining volume in the tubes was poured and filled again with 5 mL of deionized water. The cumulative drug release percentage was calculated via Eq. (3) [29–31]:

$$\text{Cumulative drug release (\%)} = \frac{Q_t}{Q_m} \times 100 \quad (3)$$

where Q_t is the amount of DOX released from the conjugates at time t and Q_m is the total amount of DOX loaded onto the hydrogels.

2.6 Characterization

2.6.1 Fourier Transform Infrared Spectroscopy (FTIR)

FTIR analysis was performed to confirm the presence of functional groups in the hydrogel samples. A Perkin Elmer spectrometer (Spectrum Two) was used for FTIR measurements. The wavelength range of 4000–400 cm^{-1} was used to record the spectra.

2.6.2 Scanning Electron Microscopy (SEM) and Energy Dispersive X-ray Spectroscopy (EDS)

The morphological properties of the hydrogels were characterized by SEM (JEOL, JMS 6060). Before SEM imaging, the samples were cryogenically shattered to create cross-sectional areas and then vacuum coated. EDS microanalysis is a technique used to describe the elemental composition of a material. An EDS microanalysis can also create a map of one or more favored chemical components of interest in a sample. The EDS equipment was used to determine the hydrogel's elemental composition (JEOL, JMS 6060). The distribution of carbon, oxygen and nitrogen atoms was mapped using the EDS technique in the hydrogel containing PVA, M and TA.

2.6.3 X-ray Diffraction (XRD)

The crystallographic characteristics of the materials and the phases they contain were specified using the XRD analysis. The XRD analyzes of the hydrogel samples were performed in the Rigaku (S D /Max 2200 LV) device at a diffraction angle between 10–90° (XRD, D/Max 2200, $\text{CuK}\alpha$ ($\lambda = 1.5418 \text{ \AA}$), 2°/min).

2.6.4 Contact Angle Measurements by Diverse Liquids (Water, Di-iodomethane, and Formamide) on Hydrogels

Contact angle measurements were performed with three different liquids (Water, Di-iodomethane, and Formamide) to determine the hydrophobic character of each hydrogel and calculate their free surface energies. The procedures performed are given below.

Sample Preparation: After drying the hydrogel samples to be measured in air, tablets with smooth surfaces were produced using a laboratory-type hydraulic manual press (MSE) to minimize the effect of roughness on the contact angle.

Preparation of the measuring liquid: Before starting the contact angle measurement, the device was calibrated, and the Hamilton micro syringe was cleaned. Then, the micro syringe was washed with the wetting liquid, and the wetting angle was measured and made ready for measurement. The syringe was placed in the chamber of the calibrated contact angle device, thus making the device ready for measurement. The "Attention Tensiometer" apparatus and the sessile drop technique were used in the tests to determine contact angle at room temperature. Using a micro syringe, the gadget drips liquids with a certain surface tension onto a solid surface. Then, using optical observation, computer analysis, and the device operator's input, the contact angle created by the liquid drop on the solid surface is determined. Deionized water, formamide, and diiodomethane were used as the wetting liquids in a contact angle goniometer (Attention optical tensiometer) with 5 μL of sessile water drops. The contact angle measurement device's software used the Acid–Base, OWRK/Fowkes, Equation of State, and Wu methods to automatically calculate the free surface energies.

2.6.5 Bioactivity Test

Biomaterials are frequently subjected to *in vivo* bioactivity testing to determine their biocompatibility. Simulated Body Fluid (SBF), which is utilized for this, mimics the biochemical conditions found in the human body to examine the biological responses of biomaterials or implants. According to the literature, the *in vitro* bioactivity of the hydrogels was evaluated in SBF following the established procedure. Salts were dissolved in 1000 mL of ultrapure water at 37 °C to create SBF solutions. After the first chemical had dissolved, the subsequent chemicals were added one at a time to generate SBF solutions. It was prepared and then buffered with TRIS and HCl to pH 7.4. By immersing the hydrogels in the produced SBF fluid at 37 °C for 14 days and observing the formation of apatite on the hydrogel surface, the hydrogels' bioactivity was assessed *in vitro*. The hydrogel's apatite formation was verified by SEM.

3 Results and Discussion

3.1 Characterization of PVA/M/TA Hydrogels

The degree of swelling of PVA-M-TA hydrogels was determined as shown in Fig. 2. The degree of swelling stabilized

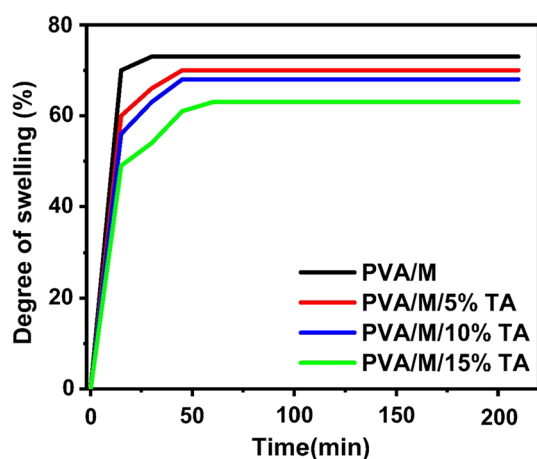


Fig. 2 Equilibrium swelling of different ratios of TA hydrogels at time intervals

after the sixtieth minute and decreased from 73% (pure PVA-M hydrogel) to 63% (PVA-M-15%TA) with increasing TA content.

The addition of TA inhibited the diffusion of water into the hydrogel by increasing the crosslink density of the hydrogel structure and reducing the pore size [32]. This effect occurs as a result of TA interacting with hydroxyl groups in the PVA matrix, increasing hydrogen bonds at the molecular level. These hydrogen bonds limit the interaction of the polymer chains with water and consequently reduce the swelling rate of the hydrogel. The increase in crosslink density reduces the solvent permeability of the polymer by linking the polymer chains together and preventing the penetration of solvent molecules into the polymer matrix. Furthermore, the increase in crosslink density leads to restricted mobility of the polymer chains due to steric effects or electrostatic interactions. This limits the penetration of solvent molecules into the polymer matrix and reduces the swelling of the hydrogel [33]. Normally, the gaps between the polymer chains allow water molecules to be retained, and therefore the hydrogel swells. However, cross-links restrict these gaps, preventing water from penetrating into the polymer matrix. This result contributes to a reduction in the swelling of the hydrogel and is in good agreement with the findings of other studies showing that TA provides a higher crosslinking density on hydrogels [34, 35].

Fourier transform infrared (FTIR) characterizations of pure PVA, M and TA and dried PVA/M/TA hydrogels were performed (Fig. 3). A Perkin Elmer spectrometer (Spectrum Two) in the 4000–400 cm^{-1} wavelength range was used for FTIR measurements. PVA has $-\text{CH}_2$, $-\text{CH}$, and $-\text{OH}$ groups with a C–C backbone and is known as a polar polymer [36]. M is a monohydrate of acetoacetic acid that forms planar chains linked by N–H...N hydrogen bonds [37]. The spectrum of the PVA/M hydrogel was found to be almost the same

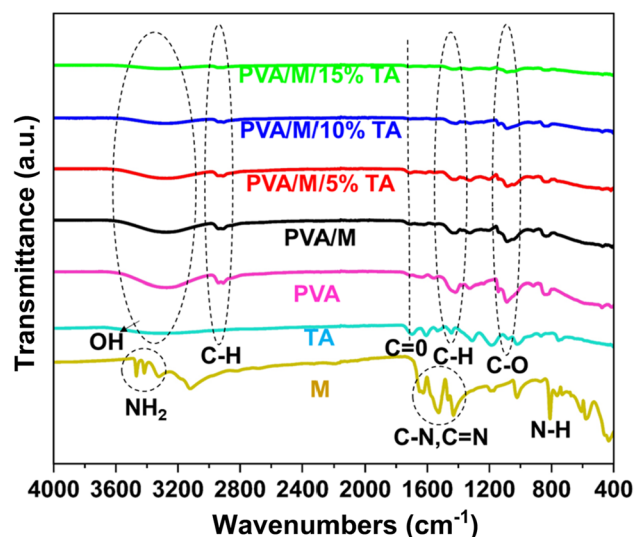


Fig. 3 FTIR spectra of hydrogels

as that of the PVA hydrogel because PVA is the main component in the hydrogel. As it can be seen in Fig. 3, in PVA/M hydrogel the peak of the $-\text{OH}$ stretching vibration shifted from 3278 cm^{-1} in PVA to 3286 cm^{-1} . The new hydrogen bond formation between the M and PVA chains is thought to be weaker than the original intramolecular hydrogen bond in PVA [38]. The broad absorption peak at about 3286 cm^{-1} in the PVA/M spectrum was attributed to the overlapping of the $-\text{OH}$ and $\text{N}-\text{H}$ stretching vibrations [39]. However, the $-\text{OH}$ stress peaks of the PVA/M/TA hydrogels at 5–15 wt% TA shifted to a lower wavenumber of 3282 cm^{-1} . The strength constants of chemical bonds can result in changes in the vibrational frequencies of these bonds to lower wavenumbers [40]. As it can be seen from Fig. 3, differences in the locations of the peaks were observed due to the interactions between the functional groups in the hydrogel samples, which confirms the affinity between the compounds. As the TA ratio increased, the intensity of the peaks belonging to the hydroxyl ($-\text{OH}$) groups in the Fig. 3 decreased. When TA binds to hydroxyl groups, it does not allow the release of hydroxyl groups, which reduces the density of the hydroxyl groups. Although changes in the intensity of the peak belonging to hydroxyl groups were observed, the presence of OH groups were confirmed by the large peak with a peak of around 3300 cm^{-1} . The bands at $2908 - 2940 \text{ cm}^{-1}$ are mainly because of PVA and appears to be due to the C–H stretching vibration attributed to the aliphatic hydrocarbon's $-\text{CH}$ and $-\text{CH}_2$ groups [23]. C = O stretching is involved in the peaks at 1708 cm^{-1} . The stretching vibrations associated with C – N, C = N, and the skeletal stretching vibrations of these aromatic rings are indicated in the band $1636\text{--}1424 \text{ cm}^{-1}$. But the M all characteristic bands practically do not appear in the sample spectra, probably because, the M content represents a rather small percentage in the samples [41]. The

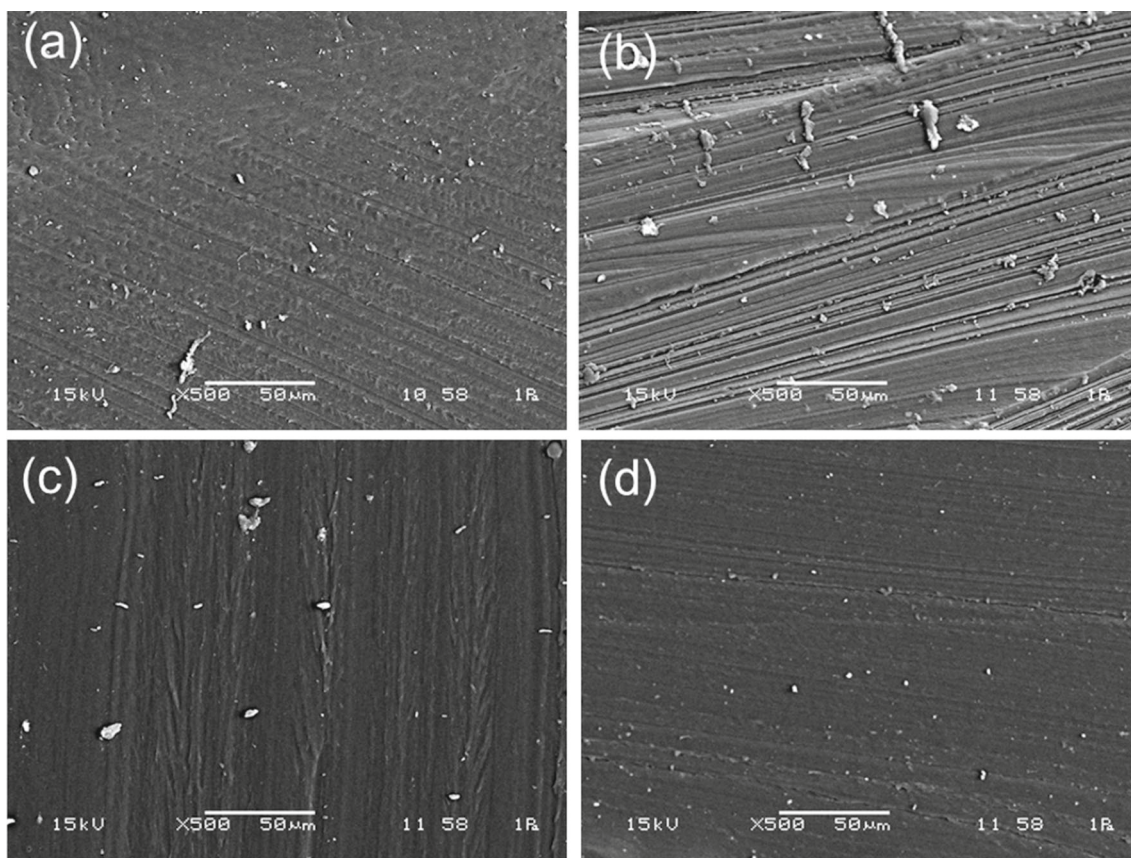


Fig. 4 SEM micrographs of **a** PVA/M hydrogel, **b** PVA/M/5%TA hydrogel, **c** PVA/M/10%TA hydrogel, **d** PVA/M/15%TA hydrogel

absorbance at 1424 cm^{-1} corresponds to the asymmetric stretching vibration peak of C–H. In alcohols, the peak at 1085 cm^{-1} can be defined as the C–O stretching peak [42]. The band $831\text{--}836\text{ cm}^{-1}$ depends on the C – NH_2 group and the ring width or bending vibration modes [43]. As a result of the FTIR analysis, it is expected that the compound will become more hydrophobic as TA reduces the density of the hydroxyl groups by bonding with the hydroxyl groups of PVA. This expectation is also supported by the contact angle.

The morphology of TA-added PVA/M hydrogels was observed by SEM (JEOL, JMS 6060) (Fig. 4). The strips are assigned to the cutting process applied before the section view. As expected, the morphological structures of the lyophilization-dried hydrogel samples, which did not contain porous structure, were obtained in accordance with the literature [44]. In addition, while it was observed that the PVA/M hydrogel showed partial aggregation in the cross-sectional image (Fig. 4a), in the PVA/M/TA matrix it was observed that aggregation decreased with increasing TA ratio (Fig. 4b–d). This can be thought to be due to the increase of hydrogen bonds with TA in the structure.

The EDS map of the hydrogel containing 5% TA was obtained and presented in Fig. 5 to confirm the homogeneity in the SEM images of the hydrogel in Fig. 4. Figure 4a

shows the SEM image of a PVA hydrogel containing M (1.5% wt.) and TA (5% wt.). This image was chosen to map carbon (Fig. 5b), oxygen (Fig. 5c), and nitrogen (Fig. 5d) atoms. The EDS mapping of the carbon, oxygen and nitrogen atoms is shown in Fig. 5b–d as colored dots, respectively. The hydrogel's existence of crucial carbon, oxygen, and nitrogen signals was confirmed by EDS (JEOL, JMS 6060) analysis. In the investigated hydrogel, carbon and oxygen can be associated with the polymeric matrix of PVA. The mapped area in this instance has a homogeneous distribution of dots, which is consistent with the SEM images in Fig. 5. The samples are composed of organic compounds and it is seen that there are mostly C, O and N atoms in terms of density, respectively.

The XRD analyzes of the hydrogel samples were performed in the Rigaku (S D /Max 2200 LV) device at a diffraction angle between $10\text{--}90^\circ$ (XRD, D/Max 2200, Cu $K\alpha$ ($\lambda = 1.5418\text{ \AA}$), $2^\circ/\text{min}$). The dried PVA hydrogels show three characteristic peaks at $2\theta = 19.6^\circ$, 22.9° , and 40.8° coinciding with the (101), (200), and (102) PVA crystallinity planes, respectively [39]. With the addition of M to the PVA hydrogel structure, these peaks were observed to be 19.26° , 22.56° , and 40.4° , respectively. The fact that there was no large difference in the diffraction peak intensity at 19.26° of the PVA hydrogels with increasing TA content indicates that

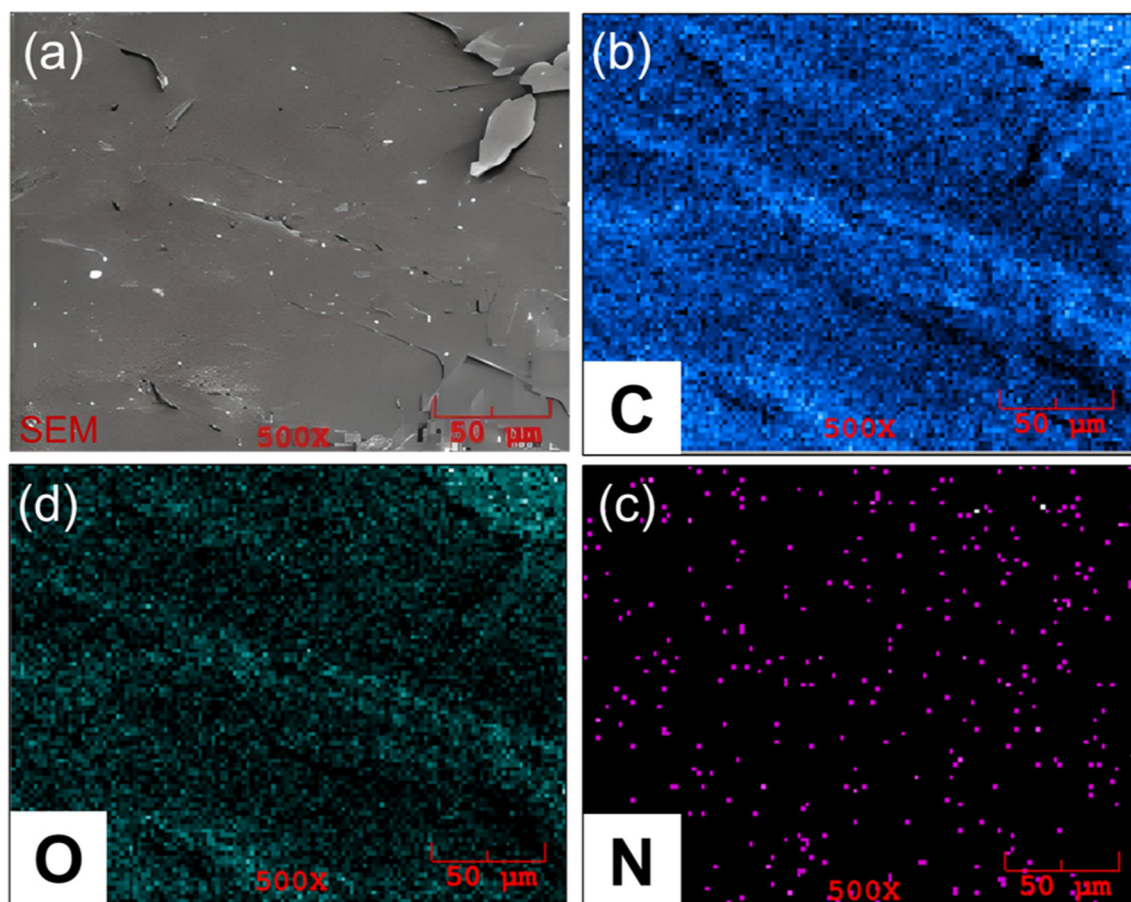


Fig. 5 SEM image of PVA-containing M (1.5% wt.) and TA (5% wt.) (a). This image was selected to map carbon (b), oxygen (c), and nitrogen (d) atoms. The colored dots in b–d represent the EDS elemental mapping of carbon, oxygen, and nitrogen atoms

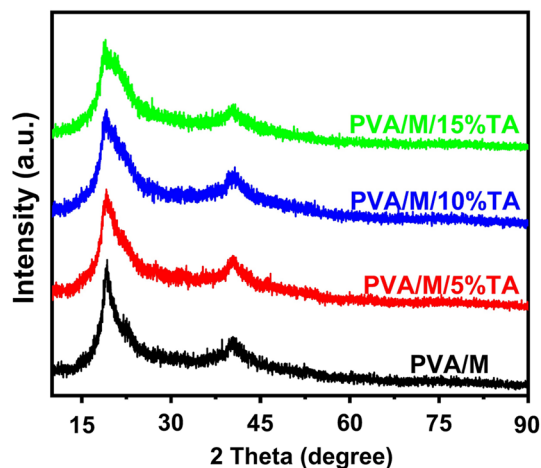


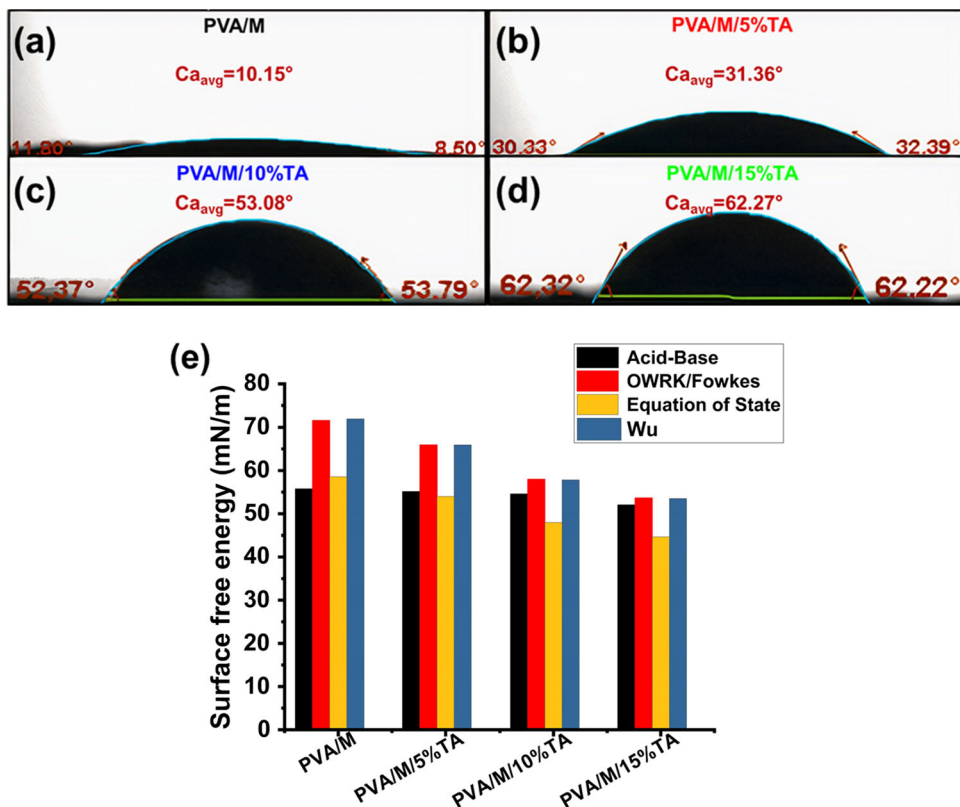
Fig. 6 XRD patterns of PVA/M/TA hydrogels

TA molecules did not change the crystal structure of PVA (Fig. 6).

According to the measurement of the contact angles in Fig. 7, the contact angle of the hydrogel without TA is 11.80°

and 8.50° (Fig. 7a), while the contact angle of the hydrogel containing 5% TA is 30.33° and 32.39° (Fig. 7b). The contact angle of the hydrogel containing 10% TA is 52.37° and 53.79° (Fig. 7c). The contact angle of the hydrogel containing 15% TA is 62.32° and 62.22° (Fig. 7d). As the TA ratio increases, the contact angle value also increases. As the contact angle increases, the hydrophobic character of the solid surface increases. As the TA ratio increased in the structure of the hydrogel, its polar nature decreased, and thus its affinity toward water decreased; that is, its hydrophobic character increased. TA has the formula $C_{76}H_{52}O_{46}$, and its structure consists of a central glucose unit esterified with gallic acid dimers [41]. TA is a plant-derived hydrolyzable active polyphenolic compound with a hydrophobic core and a hydrophilic shell of the polyphenolic structure [45]. Since TA contains hydrophobic regions, it shows hydrophobic interaction [46]. As the TA ratio in the structure of the hydrogel increased, the hydrogel's affinity for water decreased by increasing the apolar property of the hydrogel by forming hydrogen bonds with the -OH groups of PVA, which

Fig. 7 **a** 0% TA, **b** 5% TA, **c** 10% TA, **d** 15% TA hydrogels contact angle values measured with water, **e** The free surface energies of hydrogels were calculated by different



is the main component of the hydrogel, thus increasing its hydrophobic character.

Free surface energies were calculated automatically according to the Zisman, Fowkes and Van Oss Acid–Base method with the help of a computer software program in the contact angle measuring device. According to the graph in Fig. 7e, it was observed that the surface energies decrease by increasing the TA ratio of the hydrogels. Still, there are significant differences between the surface energy values calculated according to Acid–Base, Fowkes, Equation of State, and OWRK/Fowkes methods. This difference is a natural consequence of the different approaches in the calculation methods and the related mathematical equations, which are known from the literature [47]. There is an inverse relationship between hydrophobicity and free surface energy. Increasing the hydrophobic character of hydrogels reduces the free surface energy. It is known in the literature that TA has a hydrophobic or hydrophilic character because it plays different roles in different materials [70]. When we look at the results obtained after the measurement in Fig. 7e, it is seen that the hydrophobic character increases and the surface energies decrease as the TA ratio increases. As the TA ratio of the hydrogels increased, the hydrogels became more hydrophobic due to their decreased affinity for water molecules and hydrogen/hydroxyl ions. Since the bonds between molecules on the surface of the hydrogels that become hydrophobic have

been weakened and this result in a decrease in the surface free energy of hydrogels.

Prepared hydrogels were immersed in SBF solution for 14 days at 37 °C to evaluate their in vitro bioactivity. After the samples were taken out of the SBF, cleaned with distilled water, and dried, changes in the surface structure of the immersed samples were examined. The examination of the immersed samples revealed notable alterations in their surface structure, shedding light on the effects of exposure to SBF. Figure 8a shows that hydroxyapatite formation occurred on the surface of PVA/M hydrogel. In Fig. 8b, it was observed that hydroxyapatite formation was more intense on the surface of PVA/M/15%TA hydrogel. Therefore, it was observed that the addition of TA to the hydrogel increased the bioactivity of the hydrogel [48, 49].

3.2 Encapsulation Efficiency and Drug Release Manner of Hydrogels

The effect of the hydrogel on the encapsulation efficiency of increasing amounts of TA is shown in Fig. 9. DOX was physically loaded onto the hydrogel. Physical adhesion occurs due to the pore structure and hydrophilic/hydrophobic properties of the hydrogel matrix. Physical interactions such as electrostatic interactions, hydrogen bonds, and Van der Waals forces between the hydrogel matrix and drug molecules can also

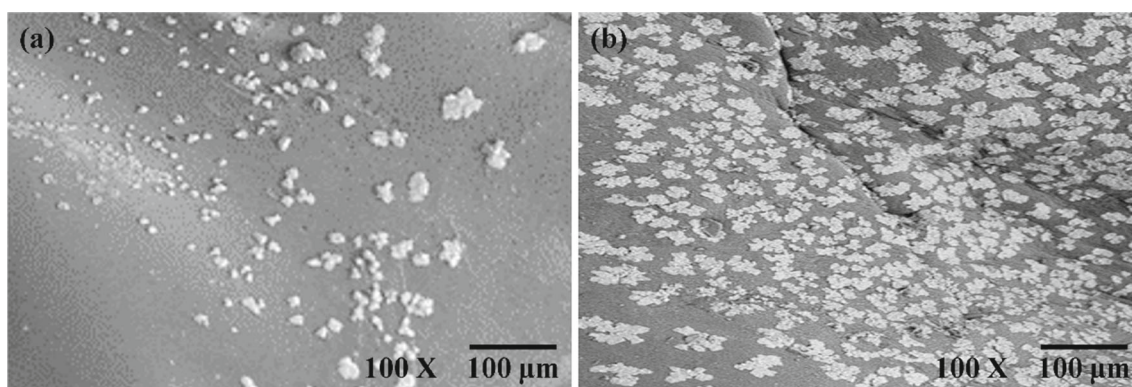


Fig. 8 Surface morphology of **a** PVA/M hydrogels and **b** PVA/M/15% hydrogels after 14 days in SBF

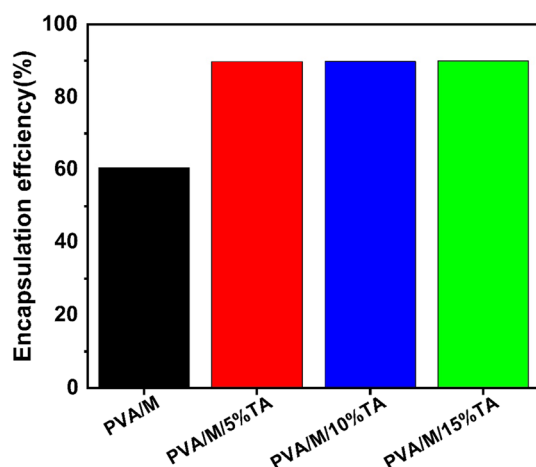


Fig. 9 The effect of varying amounts of TA on the encapsulation efficiency of the hydrogel

enhance adhesion. It is expected that as the TA ratio increases, the hydrogel becomes more resistant to attack by the surrounding water molecules by narrowing the pore size as the crosslink density increases due to the newly formed hydrogen bonds, and it is expected that the PVA/M/TA hydrogels will have better adhesion of drugs in the hydrogel, that is, higher drug encapsulation, compared to the corresponding PVA/M hydrogels [50]. As supported by the swelling analysis, TA ratio increased the encapsulation efficiency from 60 to 90% and increased by about 50% with increasing TA ratio.

The graphs in Fig. 10 show the cumulative drug release by US and under room temperature conditions without US of DOX-loaded hydrogels containing TA ratio of 0% (Fig. 10a), 5% (Fig. 10b), 10% (Fig. 10c), and 15% (Fig. 10d), respectively. The hydrophobic properties of the hydrogel, determined by the contact angle with increasing TA ratio, decrease the interaction of the polymer chains with water and do not allow water to diffuse urgently into the polymer core, thus reducing drug release by better encapsulating the drug and affecting drug release kinetics [51, 52].

Since US can change the cellular integrity of the cell membrane by temporarily disrupting the calcium cross-links, it increases the drug release as it increases the tissue's permeability [38].

In all graphs in Fig. 10, US-triggered hydrogels release more drugs than non-triggered hydrogels, increasing ultrasound duration. As the ultrasound duration increased, the cumulative drug release rates increased 3.2 times in the PVA/M hydrogel in Fig. 10a. The enhancing effect of US on drug release has been confirmed in the literature with studies using different materials such as chitosan-mesoporous silica (CS-MS), sodium alginate, poly(D,L-lactide-co-glycolide)-methoxy-poly(ethylene glycol) (PLGA-mPEG), liposome [53–55].

Since TA increases the crosslinking density by forming hydrogen bonds, it creates polymer chains with higher rigidity, thus reducing drug release by encapsulating the drug better [50, 56]. As TA catechol groups form hydrogen bonds with PVA and M and intensify intra-matrix crosslinking with the incorporation of TA into hydrogels, it is seen that when the TA ratio is increased, the drug release decreases when the graphs in Fig. 10 are compared. For example, the cumulative drug release of the PVA/M hydrogel is 27.8% for 60 min (Fig. 10a), while the cumulative drug release of the PVA/M/15% hydrogel is 22.6% (Fig. 10d) at room conditions. As TA ratios increased, drug release decreased. In US-triggered hydrogels, the cumulative drug release of the PVA/M was 60.5% while the cumulative drug release of the PVA/M/15% hydrogel was 35.4% in 60 min. Looking at the drug release graph of the hydrogel PVA/M/5% TA in Fig. 10b, the drug release for 15 minutes is 9.6% (NO US) and 17.6% (US), while for 45 min it is 23.3% (NO US) and 43.5% (US). As the duration of US use increased, drug release also increased. Drug release increased as the duration of ultrasound use increased. It was observed that the increase in US-triggered drug release was low before the addition of TA acid, increased after the addition of TA and decreased with increasing TA content. Furthermore, the drug release

Fig. 10 Cumulative drug release of a hydrogel that included **a** 0% TA, **b** 5% TA, **c** 10% TA and **d** 15% TA

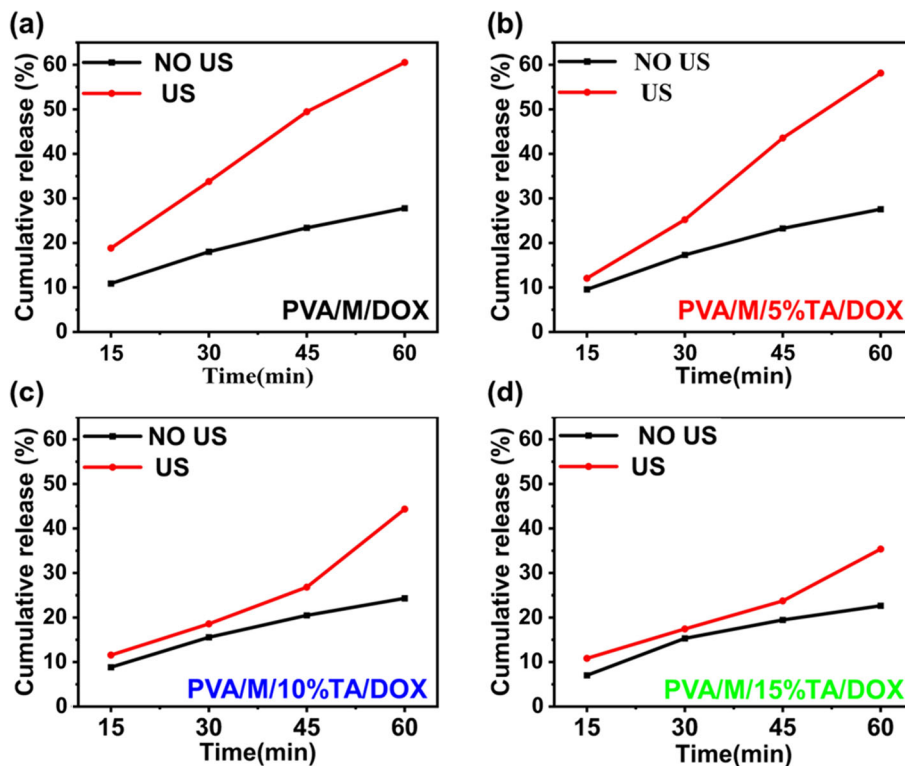


Table 1 Results of US-triggered drug release enhancement at different TA ratio

Hydrogels	Drug release increase with US (Times)
PVA/M	3.2
PVA/M/5%TA	4.8
PVA/M/10%TA	3.5
PVA/M/15%TA	3.3

in all hydrogel samples increased on average 3.7 times with increasing US time (Table 1). Looking at the hydrogel with PVA/M/10% TA in Fig. 10c, it could be seen that the release amounts with US and without US were close to each other for 45 min. Figure 10d' shows a similar release profile. The drug release can be increased by increasing the ultrasonic power. These results were found to be in agreement with the literature [57, 58].

4 Conclusion

As a result of this experiment, it is shown that it can be developed by adding materials that will provide the desired properties to the hydrogel, especially for drug release, and drug release can be controlled by the US. The TA and M materials used for this purpose are considered a good example for biomedical applications. In future studies, the formulation of

the TA and M ratios can be further investigated. In addition to these suggestions, different US frequencies can be used. It is recommended to extend the research study by increasing the duration of the samples taken for drug release and triggering the US intermittently.

The following conclusions can be drawn from the study:

- Innovative ultrasound-sensitive hydrogels have been successfully synthesized by the freeze–thaw method.
- As expected from the FTIR analysis, the hydrogel became more hydrophobic as the TA ratio increased, confirmed by a decrease in surface energy and an increase in contact angle.
- As the TA ratio increases, the swelling behavior of the hydrogel decreases as the hydrogel becomes more hydrophobic and the pore size shrinks due to the density of the newly formed hydrogen bonds; similar to this trend, the efficiency of encapsulation increases, and the drug release is successfully slowed down.
- Cross-linked DOX-loaded interpenetrating network (IPN) hydrogels have successfully demonstrated ultrasound sensitivity.
- The drug release of the successfully synthesized hydrogels increased with increasing ultrasound triggering time.
- The synthesized smart hydrogels with homogeneous morphology and adjustable properties are promising for potential applications.

Declarations

Conflict of interest The authors declare no conflicts of interest.

References

- Suresh, A.B.; Rajeev, M.R.; Anirudhan, T.S.: Synthesis of modified tannic acid hydrogel for the transdermal delivery of curcumin. *J. Environ. Chem. Eng.* **11**, 109862 (2023). <https://doi.org/10.1016/j.jece.2023.109862>
- Wang, T.-C.; Tsai, W.-B.: A biphasic mathematical model for the release of polymer-drug conjugates from poly(vinyl alcohol) hydrogels. *J. Taiwan Inst. Chem. Eng.* **135**, 104395 (2022). <https://doi.org/10.1016/j.jtice.2022.104395>
- Hughes, G.A.: Nanostructure-mediated drug delivery. *Nanomed. Nanotechnol. Biol. Med.* **1**, 22–30 (2005). <https://doi.org/10.1016/j.nano.2004.11.009>
- Rivera-Hernández, G.; Antunes-Ricardo, M.; Martínez-Morales, P.; Sánchez, M.L.: Polyvinyl alcohol based-drug delivery systems for cancer treatment. *Int. J. Pharm.* **600**, 120478 (2021). <https://doi.org/10.1016/j.IJPHARM.2021.120478>
- Omidirad, R.; Rajabi, F.H.; Farahani, B.V.: Preparation and in vitro drug delivery response of doxorubicin loaded PAA coated magnetite nanoparticles. *J. Serbian Chem. Soc.* **78**, 1609–1616 (2013)
- Hoare, T.R.; Kohane, D.S.: Hydrogels in drug delivery: progress and challenges. *Polymer* **49**, 1993–2007 (2008). <https://doi.org/10.1016/j.polymer.2008.01.027>
- Ebrahimi, R.; Salavaty, M.: Controlled drug delivery of ciprofloxacin from ultrasonic hydrogel. *E-Polymers* **18**, 187–195 (2018). <https://doi.org/10.1515/epoly-2017-0123>
- Franco, Y.L.; Vaidya, T.R.; Ait-Oudhia, S.: Anticancer and cardio-protective effects of liposomal doxorubicin in the treatment of breast cancer. *Breast Cancer Targets Ther.* **10**, 131–141 (2018). <https://doi.org/10.2147/BCTT.S170239>
- Li, G.; Yan, Q.; Xia, H.; Zhao, Y.: Therapeutic-ultrasound-triggered shape memory of a melamine-enhanced poly(vinyl alcohol) physical hydrogel. *ACS Appl. Mater. Interfaces* **7**, 12067–12073 (2015). <https://doi.org/10.1021/acsami.5b02234>
- Shi, Q.; Wu, K.; Huang, X.; Xu, R.; Zhang, W.; Bai, J.; Du, S.; Han, N.: Tannic acid/Fe³⁺ complex coated mesoporous silica nanoparticles for controlled drug release and combined chemo-photothermal therapy. *Colloids Surf. A Physicochem Eng Asp* (2021). <https://doi.org/10.1016/j.colsurfa.2021.126475>
- Baldwin, A.; Booth, B.W.: Biomedical applications of tannic acid. *J. Biomater. Appl.* **36**, 1503–1523 (2022). <https://doi.org/10.1177/08853282211058099>
- Zhu, J.-Q.; Wu, H.; Li, Z.-L.; Xu, X.-F.; Xing, H.; Wang, M.-D.; Jia, H.-D.; Liang, L.; Li, C.; Sun, L.-Y.; Wang, Y.-G.; Shen, F.; Huang, D.-S.; Yang, T.: Responsive hydrogels based on triggered click reactions for liver cancer. *Adv. Mater.* **34**, 2201651 (2022). <https://doi.org/10.1002/adma.202201651>
- Bustamante-Torres, M.; Romero-Fierro, D.; Arcentales-Vera, B.; Palomino, K.; Magaña, H.; Bucio, E.: Hydrogels classification according to the physical or chemical interactions and as stimuli-sensitive materials. *Gels* **7**, 182 (2021). <https://doi.org/10.3390/gels7040182>
- Xia, H.; Zhao, Y.; Tong, R.: Ultrasound-mediated polymeric micelle drug delivery. *Adv. Exp. Med. Biol.* **880**, 365–384 (2016). https://doi.org/10.1007/978-3-319-22536-4_20
- Chowdhury, S.M.; Abou-Elkacem, L.; Lee, T.; Dahl, J.; Lutz, A.M.: Ultrasound and microbubble mediated therapeutic delivery: underlying mechanisms and future outlook. *J. Control. Release* **326**, 75–90 (2020). <https://doi.org/10.1016/j.jconrel.2020.06.008>
- Tu, L.; Liao, Z.; Luo, Z.; Wu, Y.-L.; Herrmann, A.; Huo, S.: Ultrasound-controlled drug release and drug activation for cancer therapy. *Exploration* **1**, 20210023 (2021). <https://doi.org/10.1002/EXP.20210023>
- Kwok, C.S.; Mourad, P.D.; Crum, L.A.; Ratner, B.D.: Self-assembled molecular structures as ultrasonically-responsive barrier membranes for pulsatile drug delivery. *J. Biomed. Mater. Res.* **57**, 151–164 (2001). [https://doi.org/10.1002/1097-4636\(200111\)57:2%3c151::AID-JBM1154%3e3.0.CO;2-5](https://doi.org/10.1002/1097-4636(200111)57:2%3c151::AID-JBM1154%3e3.0.CO;2-5)
- Meissner, S.; Akepogu, J.H.; Arnet, S.M.; Dean, M.Z.; Ji, J.; Wright, G.; Harland, B.; Raos, B.; Svirskis, D.; Thakur, S.S.: Investigating the influence of ultrasound parameters on ibuprofen drug release from hydrogels. *Drug Deliv. Transl. Res.* **13**, 1390–1404 (2023). <https://doi.org/10.1007/s13346-022-01277-5>
- Wu, C.-H.; Sun, M.-K.; Kung, Y.; Wang, Y.-C.; Chen, S.-L.; Shen, H.-H.; Chen, W.-S.; Young, T.-H.: One injection for one-week controlled release: in vitro and in vivo assessment of ultrasound-triggered drug release from injectable thermoresponsive biocompatible hydrogels. *Ultrason. Sonochem.* **62**, 104875 (2020). <https://doi.org/10.1016/j.ultsonch.2019.104875>
- Waresindo, W.X.; Luthfianti, H.R.; Priyanto, A.; Hapidin, D.A.; Edikresnha, D.; Aimon, A.H.; Suciati, T.; Khairurrijal, K.: Freeze–thaw hydrogel fabrication method: basic principles, synthesis parameters, properties, and biomedical applications. *Mater. Res. Express.* **10**, 024003 (2023). <https://doi.org/10.1088/2053-1591/acb98e>
- Adelnia, H.; Ensandoost, R.; Shebbrin Moonshi, S.; Gavvani, J.N.; Vasafi, E.I.; Ta, H.T.: Freeze/thawed polyvinyl alcohol hydrogels: present, past and future. *Eur. Polym. J.* **164**, 110974 (2022). <https://doi.org/10.1016/J.EURPOLYMJ.2021.110974>
- Kim, T.H.; An, D.B.; Oh, S.H.; Kang, M.K.; Song, H.H.; Lee, J.H.: Creating stiffness gradient polyvinyl alcohol hydrogel using a simple gradual freezing-thawing method to investigate stem cell differentiation behaviors. *Biomaterials* **40**, 51–60 (2015). <https://doi.org/10.1016/j.biomaterials.2014.11.017>
- Hu, T.; Liu, Q.; Gao, T.; Dong, K.; Wei, G.; Yao, J.: Facile preparation of tannic acid-poly(vinyl alcohol)/sodium alginate hydrogel beads for methylene blue removal from simulated solution. *ACS Omega* **3**, 7523–7531 (2018). <https://doi.org/10.1021/acsomega.8b00577>
- Du, M.; Jin, J.; Zhou, F.; Chen, J.; Jiang, W.: Dual drug-loaded hydrogels with pH-responsive and antibacterial activity for skin wound dressing. *Colloids Surf. B Biointerfaces* **222**, 113063 (2023). <https://doi.org/10.1016/j.colsurfb.2022.113063>
- Kamoun, E.A.; Omer, A.M.; Abu-Shopie, M.M.; Khattab, S.N.; Ahmed, H.M.; Elbardan, A.A.: Stereopolymerized PVA-g-GMA hydrogels for biomedical applications: factors affecting hydrogel formation and bioevaluation tests. *Arab. J. Sci. Eng.* **43**, 3565–3575 (2018). <https://doi.org/10.1007/s13369-017-3054-5>
- Kumar, R.; Singh, A.; Garg, N.: Acoustic cavitation assisted hot melt mixing technique for solid lipid nanoparticles formulation, characterization, and controlled delivery of poorly water soluble drugs. *J. Drug Deliv. Sci. Technol.* **54**, 101277 (2019). <https://doi.org/10.1016/j.jddst.2019.101277>
- Wang, F.; Xu, W.; Ouyang, Y.; Zhang, L.; Liu, H.: Reversible crosslinking terpolymer shell-based mesoporous silica nanoparticles as on-off nanocarriers for pyrene-releasing application. *J. Taiwan Inst. Chem. Eng.* **91**, 578–587 (2018). <https://doi.org/10.1016/j.jtice.2018.06.013>
- Bensouiki, S.; Belaib, F.; Sindt, M.; Magri, P.; Rup-Jacques, S.; Bensouici, C.; Meniai, A.-H.: Evaluation of anti-inflammatory activity and in vitro drug release of ibuprofen-loaded nanoparticles based on sodium alginate and chitosan. *Arab. J. Sci. Eng.* **45**, 7599–7609 (2020). <https://doi.org/10.1007/s13369-020-04720-2>
- Shi, X.; Zheng, Y.; Wang, C.; Yue, L.; Qiao, K.; Wang, G.; Wang, L.; Quan, H.: Dual stimulus responsive drug release under the



- interaction of pH value and pulsatile electric field for a bacterial cellulose/sodium alginate/multi-walled carbon nanotube hybrid hydrogel. *RSC Adv.* **5**, 41820–41829 (2015). <https://doi.org/10.1039/C5RA04897D>
30. Yuan, Y.; Choi, K.; Choi, S.-O.; Kim, J.: Early stage release control of an anticancer drug by drug-polymer miscibility in a hydrophobic fiber-based drug delivery system. *RSC Adv.* **8**, 19791–19803 (2018). <https://doi.org/10.1039/C8RA01467A>
 31. Kakkar, D.; Dumoga, S.; Kumar, R.; Chuttani, K.; Mishra, A.K.: PEGylated solid lipid nanoparticles: design, methotrexate loading and biological evaluation in animal models. *MedChemComm* **6**, 1452–1463 (2015). <https://doi.org/10.1039/C5MD00104H>
 32. Dong, L.; Han, Z.; Li, X.: Tannic acid-mediated multifunctional 3D printed composite hydrogel for osteochondral regeneration. *Int. J. Bioprint.* **8**, 587 (2022). <https://doi.org/10.18063/ijb.v8i3.587>
 33. Maitra, J.; Shukla, V.K.: Cross-linking in hydrogels—a review. *Am. J. Polym. Sci.* **4**, 25–31 (2014)
 34. Yu, S.; Ji, Y.; Guo, C.; Lu, D.; Geng, Z.; Pei, D.; Liu, Q.: A dual-cross-linked hydrogel based on hyaluronic acid/gelatin tethered via tannic acid: mechanical properties' enhancement and stability control. *Iran. Polym. J.* **30**, 307–317 (2021). <https://doi.org/10.1007/s13726-020-00891-9>
 35. Ninan, N.; Forget, A.; Shastri, V.P.; Voelcker, N.H.; Blencowe, A.: Antibacterial and anti-inflammatory pH-responsive tannic acid-carboxylated agarose composite hydrogels for wound healing. *ACS Appl. Mater. Interfaces* **8**(42), 28511–28521 (2016)
 36. Karaer Yağmur, H.: Preparation and characterization of polyvinyl alcohol/activated carbon (PVA/AC) composite and its use in the adsorption of 4-nitrophenol (4-NP). *Adıyaman Univ. J. Sci.* **10**, 160–178 (2020). <https://doi.org/10.37094/adyujsci.628399>
 37. Marchewka, M.K.: 2,4,6-Triamino-1,3,5-triazin-1-ium acetate acetic acid solvate monohydrate. Infrared and Raman spectra. *Bull. Korean Chem. Soc.* **25**, 466–470 (2004)
 38. Cui, S.; Li, L.; Wang, Q.: Enhancing glass transition temperature and mechanical properties of poly(propylene carbonate) by intermacromolecular complexation with poly(vinyl alcohol). *Compos. Sci. Technol.* **127**, 177–184 (2016). <https://doi.org/10.1016/j.compscitech.2016.03.007>
 39. Liao, H.; Liu, Y.; Wang, Q.; Duan, W.: Preparation and properties of a poly(vinyl alcohol) hydrogel-melamine formaldehyde foam composite. *Polym. Compos.* **40**, 2067–2075 (2019). <https://doi.org/10.1002/pc.24988>
 40. Chen, Y.N.; Jiao, C.; Zhao, Y.; Zhang, J.; Wang, H.: Self-assembled polyvinyl alcohol-tannic acid hydrogels with diverse microstructures and good mechanical properties. *ACS Omega* **3**, 11788–11795 (2018). <https://doi.org/10.1021/acsomega.8b02041>
 41. Aelenei, N.; Popa, M.I.; Novac, O.; Lisa, G.; Balaita, L.: Tannic acid incorporation in chitosan-based microparticles and in vitro controlled release. *J. Mater. Sci. Mater. Med.* **20**, 1095–1102 (2009). <https://doi.org/10.1007/s10856-008-3675-z>
 42. Kenawy, E.-R.S.; Kamoun, E.A.; Ghaly, Z.S.; Shokr, A.M.; El-Meligy, M.A.; Mahmoud, Y.A.-G.: Novel physically cross-linked curcumin-loaded PVA/aloe vera hydrogel membranes for acceleration of topical wound healing: in vitro and in vivo experiments. *Arab. J. Sci. Eng.* **48**, 497–514 (2023). <https://doi.org/10.1007/s13369-022-07283-6>
 43. Marchewka, M.K.: Infrared and Raman spectra of melaminium chloride hemihydrate. *Mater. Sci. Eng.* **95**, 214–221 (2002). [https://doi.org/10.1016/S0921-5107\(02\)00235-0](https://doi.org/10.1016/S0921-5107(02)00235-0)
 44. Kaur, T.; Thirugnanam, A.; Pramanik, K.: Tailoring the in vitro characteristics of poly(vinyl alcohol)-nanohydroxyapatite composite scaffolds for bone tissue engineering. *J. J. Polym. Eng.* **36**, 771–784 (2016). <https://doi.org/10.1515/polyeng-2015-0252>
 45. Guler, T.; Polat, E.: Tannic acid as a hydrophobic modifier for galena in the presence of metal ions. *Physicochem. Probl. Miner. Process.* **53**, 5–16 (2017). <https://doi.org/10.5277/ppmp170101>
 46. Oh, H.I.; Hoff, J.E.; Armstrong, G.S.; Haff, L.A.: Hydrophobic interaction in tannin-protein complexes. *J. Agric. Food Chem.* **28**, 394–398 (1980). <https://doi.org/10.1021/jf60228a020>
 47. Onishchenko, D.A.: Analytical approach to the calculation of the design values of the loads associated with discrete ice features. In: POAC'09: Proceedings of the 20th International Conference on Port and Ocean Engineering under Arctic Conditions. pp. 1013–1023 (2009)
 48. Kaczmarek, B.; Milek, O.; Michalska-Sionkowska, M.; Zasada, L.; Twardowska, M.; Warzyńska, O.; Kleszczyński, K.; Osyczka, A.M.: Novel eco-friendly tannic acid-enriched hydrogels-preparation and characterization for biomedical application. *Materials* **13**, 4572 (2020). <https://doi.org/10.3390/ma13204572>
 49. Guo, J.; Tian, X.; Xie, D.; Rahn, K.; Gerhard, E.; Kuzma, M.L.; Zhou, D.; Dong, C.; Bai, X.; Lu, Z.; Yang, J.: Citrate-based tannin-bridged bone composites for lumbar fusion. *Adv. Funct. Mater.* **30**, 2002438 (2020). <https://doi.org/10.1002/adfm.202002438>
 50. Abulatefeh, S.R.; Taha, M.O.: Enhanced drug encapsulation and extended release profiles of calcium-alginate nanoparticles by using tannic acid as a bridging cross-linking agent. *J. Microencapsul.* **32**, 96–105 (2015). <https://doi.org/10.3109/02652048.2014.985343>
 51. Saidi, M.; Dabbaghi, A.; Rahmani, S.: Swelling and drug delivery kinetics of click-synthesized hydrogels based on various combinations of PEG and star-shaped PCL: influence of network parameters on swelling and release behavior. *Polym. Bull.* **77**, 3989–4010 (2020). <https://doi.org/10.1007/s00289-019-02948-z>
 52. Gharehnozifam, Z.; Dolatabadi, R.; Baniassadi, M.; Shahsavari, H.; Kajbafzadeh, A.M.; Abrinia, K.; Gharehnozifam, K.; Baghani, M.: Multiphysics modeling and experiments on ultrasound-triggered drug delivery from silk fibroin hydrogel for Wilms tumor. *Int. J. Pharm.* **621**, 121787 (2022). <https://doi.org/10.1016/J.IJPHARM.2022.121787>
 53. Epstein-Barash, H.; Orbey, G.; Polat, B.E.; Ewoldt, R.H.; Feshitan, J.; Langer, R.; Borden, M.A.; Kohane, D.S.: A microcomposite hydrogel for repeated on-demand ultrasound-triggered drug delivery. *Biomaterials* **31**, 5208–5217 (2010). <https://doi.org/10.1016/j.biomaterials.2010.03.008>
 54. Depan, D.; Saikia, L.; Singh, R.P.: Ultrasound-triggered release of ibuprofen from a chitosan-mesoporous silica composite—a novel approach for controlled drug release. *Macromol. Symp.* **287**, 80–88 (2010). <https://doi.org/10.1002/masy.201050111>
 55. Du, L.; Jin, Y.; Zhou, W.; Zhao, J.: Ultrasound-triggered drug release and enhanced anticancer effect of doxorubicin-loaded poly(D,L-lactide-co-glycolide)-methoxy-poly(ethylene glycol) nanodroplets. *Ultrasound Med. Biol.* **37**, 1252–1258 (2011). <https://doi.org/10.1016/j.ultrasmedbio.2011.05.012>
 56. Sun, W.; Jiang, H.; Wu, X.; Xu, Z.; Yao, C.; Wang, J.; Qin, M.; Jiang, Q.; Wang, W.; Shi, D.; Cao, Y.: Strong dual-crosslinked hydrogels for ultrasound-triggered drug delivery. *Nano Res.* **12**, 115–119 (2019). <https://doi.org/10.1007/s12274-018-2188-4>
 57. Hussein, G.A.; Myrup, G.D.; Pitt, W.G.; Christensen, D.A.; Rapoport, N.Y.: Factors affecting acoustically triggered release of drugs from polymeric micelles. *J. Control. Release* **69**(1), 43 (2000)
 58. Qin, H.; Teng, R.; Liu, Y.; Li, J.; Yu, M.: Drug release from gelsolin-targeted phase-transition nanoparticles triggered by low-intensity focused ultrasound. *Int. J. Nanomed.* **17**, 61–71 (2022). <https://doi.org/10.2147/IJN.S341421>

Springer Nature or its licensor (e.g. a society or other partner) holds exclusive rights to this article under a publishing agreement with the author(s) or other rightsholder(s); author self-archiving of the accepted manuscript version of this article is solely governed by the terms of such publishing agreement and applicable law.

